Journal Pre-proof

Fabrication of the Ni/ZnO/BiOI foam for the improved electrochemical biosensing performance to glucose

Minggang Zhao, Jinghua Shang, Huiyan Qu, Rongjie Gao, Hui Li, Shougang Chen

PII: S0003-2670(19)31258-9

DOI: https://doi.org/10.1016/j.aca.2019.10.033

Reference: ACA 237167

To appear in: *Analytica Chimica Acta*

Received Date: 14 August 2019

Revised Date: 15 October 2019

Accepted Date: 16 October 2019

Please cite this article as: M. Zhao, J. Shang, H. Qu, R. Gao, H. Li, S. Chen, Fabrication of the Ni/ZnO/BiOI foam for the improved electrochemical biosensing performance to glucose, *Analytica Chimica Acta*, https://doi.org/10.1016/j.aca.2019.10.033.

Graphical Abstract

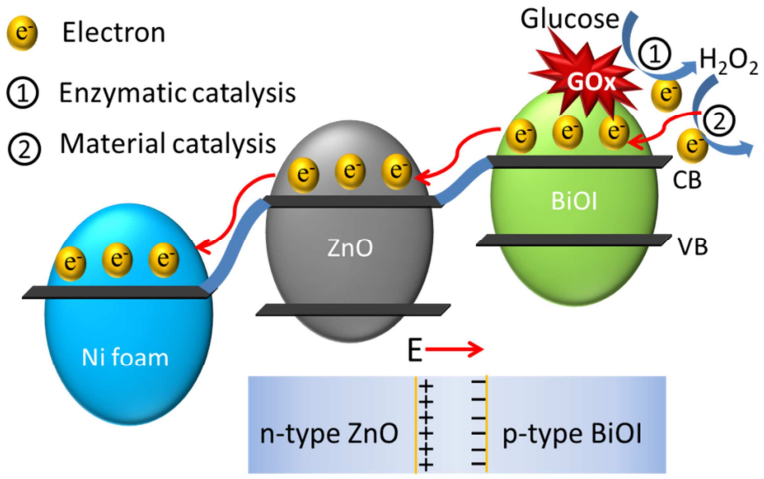

Fabrication of the Ni/ZnO/BiOI foam for the improved electrochemical biosensing performance to glucose

Minggang Zhao[a], Jinghua Shang[a], Huiyan Qu[a], Rongjie Gao [a,], Hui Li[b], Shougang Chen[a,]**

[a]*School of Materials Science and Engineering, Ocean University of China, 266100, Qingdao, Peoples R China*

[b]*Optoelectronic Materials and Technologies Engineering Laboratory of Shandong, Physics Department, Qingdao University of Science and Technology, Qingdao 266100, PR China*

Abstract

The Ni foam decorated with ZnO/BiOI core-shell p-n junction nanorods was prepared and employed as an enzyme loading matrix to detect glucose. The detection potential was decreased significantly (0.3 V) and the sensitivity was enhanced largely (115.2 $\mu A \cdot mM^{-1} \cdot cm^{-2}$). The metal-semiconductor foam can afford the porous surface for loading enzymes and achieving the multiple catalysis. More important, the built-in electric field and electron well in the p-n junction interface provide the driving force for electron transport. It was an effective strategy to enhance the biosensing performance by the rational design of p-n junction.

Keywords: semiconductor, electrochemical, foam, p-n junction, biosensor

*E-mail: zhaomg@ouc.edu.cn

1. Introduction

Glucose detection is an extensively studied subject due to its great value in environmental monitoring, food analysis, biological process monitoring, medical diagnosis and biotechnology diabetes management. Intense focus has been paid to develop the effective and reliable sensors to detect glucose, for example, electrochemical method, optical method, colorimetry and fluorescent spectroscopy [1-6]. Among them, electrochemical method has caused widespread concern on account of the simplicity, high-sensitivity and excellent repeatability [7-8]. The amperometric enzymatic glucose sensors, which are an important branch of electrochemical sensors, have the characteristics of high sensitivity and fast response. However, the applied potential is usually around 0.8 V. The high applied potential is easy to trigger the interference of electroactive substance and cause the poor selectivity. Generally speaking, the lower applied potential can reduce the interference of electroactive substance and improve the selectivity. Hence, it is urgent to find a novel sensing material as enzymes loading matrix to decrease the applied potential of electrochemical sensors.

Previous reports have indicated that the oxidation initiation potential primarily determined by the energy barrier controlled by the active sites and electron transport. [9]. As for the enzymatic glucose biosensors, the active sites include two aspects, one is the catalytic effect of glucose oxidase (GOx) on glucose, and the other is the catalytic effect of the electrode material on H_2O_2. On one hand, the catalytic activity of the denatured GOx is reduced and leads to the poor sensing performance, so it is

vital to achieve the effective immobilization of enzymes [10-11]. Previous reports have demonstrated the metal oxide nanostructures with the unique morphology could help sustain the low leaching, high loading, well stability and the improved activity of enzymes [12]. Especially, the nanopore would prominently enlarge the surface area of enzyme and offer a unique environment for maintaining the enzymatic activity. [13]. Therefore, it is helpful for the effective immobilization of enzymes by fabricating porous metal oxides nanostructures with special morphology. On the other hand, the catalysis of H_2O_2 that produced by GOx catalyzing glucose is another factor to enhance the sensing performance [14]. Heavy metals, such as Au and Pt, have efficient catalytic ability to H_2O_2, but the high cost and biotoxicity limit their applications. Some semiconductors, such as NiO and Co_3O_4, were shown to have the catalytic activity towards H_2O_2, but the poor conductivity hindered the electron transport and decelerated the redox reaction [15]. Therefore, it is expected to fabricate an electrode material with the efficient enzyme immobilization, the high catalysis towards H_2O_2 and the excellent electron transfer ability.

Recently, construction of heterostructure interfaces has attracted tremendous attention in developing new sensors. For instance, p-n junction formed by ZnO/NiO combined with single kinky nanowire to detect protein [16]. P-n junction is well known as its unique interfacial electronic state resulting from the special energy band structure. The built-in electric field formed by the p-n junction space charges region can offer the power for electron transferring from the p-type semiconductor to the n-type semiconductor, so the electron transfer can be accelerated. For example, the

p-n junction accelerates the separation of photon generation carriers, which can achieve the improved photocatalytic efficiency [17]. Similarly, the driving force can also be used to accelerate the enzyme-catalyzed electron transfer, which is helpful to enhance the biosensing performance. Hence, it's expected to fabricate the p-n junction nanostructures as the loading matrix for enzymatic sensors.

Bismuth oxyhalides BiOX (X = Cl, Br, I), a p-type semiconductor, has great influences on its optical and electrical performances and has broad application prospects in pigments, pharmaceuticals, catalysts and gas sensors [18]. Since the $[Bi_2O_2]$ plate is interdigitated with the double-layer halogen atom layer in the [001] direction to form a special layered structure, the internal electrostatic field between the anion halogen layers and the $[Bi_2O_2]^{2+}$ contributes to the improvement of the catalytic ability [19]. Recently, BiOI has aroused people's interest in application of optoelectronic device and different structures are prepared [20-21]. ZnO is an n-type semiconductor with many merits such as nontoxicity, high electron mobility, high Isoelectric Point and biocompatibility [22-24]. ZnO nanomaterials have been applied extensively in solar cells, photocatalyst and chemical sensors. Previous work demonstrated that the construction of ZnO/BiOI p-n junctions could improve the dynamic and photocatalytic performances of photogenerated carriers [25], so it is desired to develop its biosensing performance by using it as the enzymes loading matrix.

Herein, the ZnO/BiOI core-shell p-n junction nanorod with porous surface was favourably prepared on Ni foam. The 3D porous structure was employed as an

enzyme loading matrix to fix GOx for glucose detection, and the low detection potential (0.3 V), the excellent sensitivity (115.2 $\mu A \cdot mM^{-1} \cdot cm^{-2}$) and the good selectivity were obtained. The influence of p-n junction on the biosensing performance of the enzymatic glucose biosensor was discussed. It is found the strong catalysis to H_2O_2 and the accelerated electrons transport ability are important for enhancing the biosensing performance.

2. Material and methods

2.1 Synthesis of the 3D Ni/ZnO foam

ZnO nanorod was prepared by a classical hydrothermal method [26]. The Ni foam was cut and ultrasonically washed with acetone, alcohol and deionized (DI) water for 15 min, respectively. Whereafter, it was dried with N_2 flow. Then, 0.416 g $Zn(NO_3)_2 \cdot 6H_2O$ was added into 38 mL DI water under stirring to form a clear solution. Next, 2 mL $NH_3 \cdot H_2O$ was added dropwise to the precursor solution and mixed for 10 min. The final solution was introduced into an autoclave containing Ni foam and heated to 95 °C for 3 h. Ultimately, the foam was douched and dried.

2.2 Synthesis of the 3D Ni/ZnO/BiOI foam

First, 36.4 mg $Bi(NO_3)_3 \cdot 5H_2O$ was added into 20 mL ethylene glycol monomethyl ether under stirring. Then, the corresponding proportional KI was added with stirring to form the precursor solution, which was poured into the autoclave containing the 3D Ni/ZnO foam. Then, the autoclave was treated at 120 ℃ for 6 h. Finally, the foam was cooled down, cleaned by DI water and dried.

2.3 Fabrication of the enzymatic biosensor

The glassy carbon electrode (GCE) (diameter ~ 3 mm) was polished with alumina, and the electrode was ultrasonically treated with ethanol and DI water, respectively. The GOx based electrode was fabricated by chitosan-assisted cross-linking technique. 10 $mg \cdot mL^{-1}$ enzymes solution was obtained by adding GOx in 0.1 M phosphate buffer saline (PBS, pH=7.4). Chitosan solution with the concentration of 0.5 wt.% was obtained by adding chitosan in acetic acid. First, GOx solution was dropped onto the Ni/ZnO/BiOI foam (4×4 mm) and then putted in the air to dry. After drying, chitosan solution was added dropwise on the electrode to stop the spillage of GOx. The final enzymatic electrode was dried and preserved at 4 ℃ for use.

2.4. Characterization and electrochemical measurement

The structure of sample was obtained by S-4800 scanning electron microscope (SEM) and HITACHIH-7650 transmission electron microscope (TEM). The X-ray diffraction (XRD) pattern of the samples was characterized by a Bruker D8 ADVANCE X-ray diffractometer with Cu Kα radiation. Energy Dispersive Spectra (EDS) was obtained by S-4800 SEM. The biosensing tests were performed in 0.1 M PBS with a CHI600E workstation (Shanghai Chenhua). The typical three-electrode system was used, which includes platinum (Pt) electrode as counter electrode, Ag/AgCl electrode as reference electrode and Ni/ZnO/BiOI foam modified GCE as working electrode.

3. Result and discussion

3.1 Characterization of the 3D Ni/ZnO/BiOI foam

The morphology and structure of the 3D Ni/ZnO/BiOI foam are shown in **Fig. 1**.

From **Fig. 1a-c,** it is found that the ZnO nanorods grow uniformly on the Ni foam with the 3D porous structure, which has a needle-like structure with the tip about 200-500 nm wide and the bottom about 2-3 μm wide. From **Fig. 1d-f**, we can see that the surface of the foam becomes rougher after the secondary growth of BiOI nanoshell. The surface of the ZnO nanorods are overlay by a layer of BiOI wrinkles with the width of the wrinkles about 200-300 nm and the pores about 100-200 nm. The small nanopores are favorable to immobilize enzymes with good activity and stability [13]. From **Fig. 1g**, it is observe that the thickness of the BiOI shell is about 500 nm. TEM image further reveals the detailed structure of the BiOI shell. It is observed that the wrinkles on the surface consist of many BiOI nanosheets (**Fig. 1h**). The schematic diagram is shown in **Fig. 1i**, it is a combination of Ni foam and p-n junction, which forms a favorable pathway for electrons transport from p-n junction to Ni foam. The p-n junction consists of p-type BiOI as the shell and n-type ZnO as the core. The detailed process for immobilizing GOx is illustrated in **Scheme 1**. GOx molecules are adsorbed into the porous BiOI shell by the electrostatic adsorption and the physical action of porous structures. Chitosan then protects GOx by coating the outer surface of the nanorod with a permeable membrane. The trapped immobilization is stable and the nanopores are beneficial to keep the enzymatic activity.

The crystal structure of the sample was investigated by XRD (**Fig. S1**.). The strongest diffraction peaks belong to Ni, which is the main component as the supporting matrix. The second strong diffraction peaks correspond to the (100), (110), (112), (101), (102), (103), (002) reflections of the hexagonal ZnO crystalline phase

with a wurtzite structure (JCPDS card No. 36-1451). The other diffraction peaks correspond to the (102), (200), (220) reflections of the tetragonal phase of BiOI [27]. The EDS element mapping image verifies that the Bi, Ni, Zn, I, and O elements coexist and are evenly distributed (**Fig. S2**).

3.2. Biosensing performance

The biosensing performance of the sample is tested by cyclic voltammetry (CV) in 0.1 M PBS (pH=7.4). As shown in **Fig. 2a,** the oxidation peak current enhances significantly after the addition of glucose, indicating the strong catalytic oxidation toward glucose. The corresponding potential of the oxidation peak is found at 0.3 V, which is lower than many previously reported works (**Table 1**). The amperometric response to glucose was carried out for further evaluation of the biosensing performance. **Fig. 2c** shows the typical i-t curve of the sample at 0.3 V, with the gradual injecting of glucose the current enhanced rapidly and reached a steady state current within 5 s. The calibration curve of glucose concentration versus current is shown in **Fig. 2d**, whose regression equation is: I (μA) = 9.83206C (mM) + 8.70375 (R^2 = 0.99419). The liner range is from 0.01 to 3.25 mM. The sensitivity is 115.2 $\mu A \cdot mM^{-1} \cdot cm^{-2}$, which is much higher than previous works (**Table 1**). The detection limit is 2 μM (based on the signal-to-noise ratio of 3). Contrast experiments were carried out, the single ZnO or BiOI grown on the Ni foam exhibited low sensitivities (ZnO 60.5 $\mu A \cdot mM^{-1} \cdot cm^{-2}$, BiOI 75.1 $\mu A \cdot mM^{-1} \cdot cm^{-2}$) and the high applied potential (around 0.6 V). The results demonstrated the formation of p-n junction improved biosensing performance.

The selectivity as an essential indicator for evaluating biosensing performance, the common interfering substances in the blood environment were detected by adding choline chloride (CC), uric acid (UA), dopamine (DA) and ascorbic acid (AA). From **Fig. 2b**, it is observed that the addition of 5 times concentration of interferent only caused negligible response, indicating the excellent selectivity to glucose. The excellent selectivity resulted from the well immobilization of GOx enzymes that had selective catalysis to glucose, demonstrating the 3D Ni/ZnO/BiOI foam was suitable for using as enzymes loading matrix. The stability of the sample was assessed by continuous cyclic scans, and only negligible changes of the current response were produced after 10 cyclic scans. The long-term stability was studied by measuring the CV response to glucose every two days for two weeks, more than 80% of the activity remained. The good stability is due to the powerful 3D integrated foam structure and the porous surface of BiOI providing a stable microenvironment for enzyme fixation. Different batches of the prepared electrodes were used for detection of glucose, and the relative standard deviation (RSD) was about 6 %, indicating the well reproducibility. The practical detection was carried out in the real serum sample by the standard addition method, and the RSD was less than 5 % (**Table S1**).

3.3. The p-n junction effects

For further analysis of the biosensing mechanism, the catalytic ability of the sample to H_2O_2 was revealed by amperometric response at 0.3 V. From **Fig 2e**, the steady-state rapidly achieved and the current enhanced after the addition of H_2O_2. As shown in **Fig. S3**, the excellent sensitivity and fast response indicate the good

catalytic activity to H_2O_2, which may come from peroxidase mimetics properties of BiOI [28]. Therefore, the biosensing process is a two-step catalytic process. H_2O_2 was first produced by GOx catalyzing glucose and then was further catalyzed by the loading electrode material (**Fig 2f)**, which would lower the obstacles of glucose redox process and produce more electrons to enhance the sensitivity [22, 29-30]. According to the energy band position vs NHE [31], Fermi level of p-type BiOI is close to the valence band, but the Fermi level of n-type ZnO is close to the conduction band. When they contacted and formed the p-n heterojunction, the Fermi level of BiOI will shift upward and that of ZnO will shift downward to achieve an equilibrium [32]. Electrons transfer from n-ZnO to p-BiOI as they contacted each other to form p-n junction, which forming positive charges and negative charges accumulation in p-BiOI and n-ZnO contact regions. [25]. At the same time, the internal electric field directed from n-ZnO to p-BiOI is established to prevent charges diffusion until the Fermi level of BiOI and ZnO reaches equilibrium. Meanwhile, E_{VB} and E_{CB} of BiOI are both more negative than those of ZnO [31, 33], and the energy band bending occurs with ZnO shifting downward and BiOI shifting upward along with the Fermi level in this process. As shown in **Fig. 3**, the bended energy bands form an electron well to extract the reactive electrons from BiOI to ZnO. In addition, the internal built-in electric field located at the p-n junction region is able to provide the power to accelerate electrons diffuse from BiOI to ZnO. Both are helpful to decrease the obstruction of glucose redox, which facilitates reduce of the applied potential. Moreover, the Ni foam can afford the porous architecture for reaction diffusion and

the integrated pathway for electron transport, which provides the basic guarantee for the efficient catalysis. Therefore, it is the p-n junction effects combined with the structure of the Ni foam that enhances the biosensing performance, including the decreased oxidation potential and the enhanced sensitivity.

4. Conclusion

In summary, we fabricated the ZnO/BiOI core-shell p-n junction ornamented Ni foam to fix GOx for glucose detection. The enhanced sensitivity (115.2 $\mu A \cdot mM^{-1} \cdot cm^{-2}$) and the decreased detection potential (0.3 V) were achieved. The electrode material combines the merits of the 3D porous metal foam and the p-n junction impacts, including the second catalysis and the accelerated electrons transport. It is a useful strategy to introduce the p-n junction effects into the enzyme loading matrix to enhance the electrochemical biosensing performance.

Acknowledgements

This work was sponsored by National Natural Science Foundation of China (51602298), Fundamental Research Funds for the Central University (841964011), Higher Educational Science and Technology Program of Shandong Province(J18KA311).

Reference

[1] S. Mross, S. Pierrat, T. Zimmermann, M. Kraft, Microfluidic enzymatic biosensing systems: A review, Biosen. Bioelectron. 70 (2015) 376-391.

[2] M.G. Zhao, J.Y. Huang, Y. Zhou, Q. Chen, X.H. Pan, H.P. He, Z.Z. Ye, A single mesoporous ZnO/Chitosan hybrid nanostructure for a novel free nanoprobe type

biosensor, Biosen. Bioelectron. 43 (2013) 226-230.

[3] J. Liao, S. Lin, Y. Yang, K. Liu, W. Du, Highly selective and sensitive glucose sensors based on organic electrochemical transistors using TiO_2 nanotube arrays-based gate electrodes, Sens. Actuators, B: Chem. 208 (2015) 457-463.

[4] S. Fan, M. Zhao, L. Ding, Y. Ma, J. Liang, X. Wang, Introducing p-n junction interface into enzyme loading matrix for enhanced glucose biosensing performance, Sens. Actuators, B: Chem. 237 (2016) 373-379.

[5] X. Gu, H. Wang, Z.D. Schultz, J.P. Camden, Sensing Glucose in Urine and Serum and Hydrogen Peroxide in Living Cells by Use of a Novel Boronate Nanoprobe Based on Surface-Enhanced Raman Spectroscopy, Anal. Chem. 88 (2016) 7191-7197.

[6] M.G. Zhao, J.Y. Huang, Y. Zhou, X.H. Pan, H.P. He, Z.Z. Ye, X.H. Pan, Controlled synthesis of spinel $ZnFe_2O_4$ decorated ZnO heterostructures as peroxidase mimetics for enhanced colorimetric biosensing, Chem. Commun. 49 (2013) 7656.

[7] M. Lin, M.S. Cho, W.S. Choe, Y. Lee, Electrochemical analysis of copper ion using a Gly-Gly-His tripeptide modified poly(3-thiopheneacetic acid) biosensor, Biosens. Bioelectron. 25 (2009) 28-33.

[8] I. Dumitrescu, J.P. Edgeworth, P.R. Unwin, J.V. Macpherson, Ultrathin Carbon Nanotube Mat Electrodes for Enhanced Amperometric Detection, Adv. Mater. 21 (2009) 3105-3109.

[10] A. Riklin, E. Katz, I. Wiliner, A. Stocker, A.F. Bückmann, Improving enzyme-electrode contacts by redox modification of cofactors, Nature 376 (1995)

672-675.

[11] E. Lima-Fernandes, S. Misticone, C. Boularan, J.S. Paradis, H. Enslen, P.P. Roux, M. Bouvier, G.S. Baillie, S. Marullo, M.G.H. Scott, A biosensor to monitor dynamic regulation and function of tumour suppressor PTEN in living cells, Nat. Commun. 5 (2014) 4431.

[12] L.J. Pan, D.Y. Yu, D.Y. Zhai, H.R. Lee, W.T. Zhao, N. Liu, H.L. Wang, B.C.K. Tee, Y. Shi, Y. Cui, Z.N. Bao, Hierarchical nanostructured conducting polymer hydrogel with high electrochemical activity, P. Natl. Acad. Sci. 109 (2012) 9287-9292.

[13] M.G. Zhao, Z. Li, Z. Han, K. Wang, Y. Zhou, J.Y. Huang, Z.Z. Ye, Synthesis of mesoporous multiwall ZnO nanotubes by replicating silk and application for enzymatic biosensor, Biosen. Bioelectron. 49 (2013) 318-322.

[14] D. Bai, Z. Zhang, K. Yu, Synthesis, field emission and glucose-sensing characteristics of nanostructural ZnO on free-standing carbon nanotubes films, Appl. Surf. Sci. 256 (2010) 2643-2648.

[15] H. Duan, D. Xu, W. Li, H. Xu, Study of the redox properties of noble metal/Co_3O_4 by electrical conductivity measurements, Catal. Lett. 124 (2008) 318-323.

[16] M.G. Zhao, B. Cai, Y. Ma, H. Cai, J.Y. Huang, X.H. Pan, H.P. He, Z.Z. Ye, Introducing heterojunction barriers into single kinked nanowires for the probe-free detection of proteins and intracellular recording, Nanoscale 6 (2014) 4052-4057.

[17] B. Lu, S. Zeng, C. Li, Y. Wang, X. Pan, L. Zhang, H. Mao, Y. Lu, Z. Ye,

Nanoscale p-n heterojunctions of BiOI/nitrogen-doped reduced graphene oxide as a high performance photocatalyst, Carbon 132 (2018) 191-198.

[18] H. Cheng, B. Huang, Y. Dai, Engineering BiOX (X = Cl, Br, I) nanostructures for highly efficient photocatalytic applications, Nanoscale 6 (2014) 2009-2026.

[19] B. Li, X. Chen, T. Zhang, S. Jiang, G. Zhang, W. Wu, X. Ma, Photocatalytic selective hydroxylation of phenol to dihydroxybenzene by BiOI/TiO_2 p-n heterojunction photocatalysts for enhanced photocatalytic activity, Appl. Surf. Sci. 439 (2018) 1047-1056.

[20] Q. Wang, Q. Guo, H. Wu, Y. Fan, D. Lin, Q. He, Y. Zhang, W. Cong, In situ construction of semimetal Bi modified BiOI-Bi_2O_3 film with highly enhanced photoelectrocatalytic performance, Sep. Purif. Technol. 226 (2019) 232-240.

[21] L. ParamanikK, H. ReddyK, M. Parida, Stupendous Photocatalytic Activity of p-BiOI/n-PbTiO3 Heterojunction: The Significant Role of Oxygen Vacancies and Interface Coupling, J. Phys. Chem. C. 123 (2019) 21593-21606.

[22] L. Luo, F. Li, L. Zhu, Y. Ding, Z. Zhang, D. Deng, B. Lu, Nonenzymatic glucose sensor based on nickel(II)oxide/ordered mesoporous carbon modified glassy carbon electrode, Colloids Surf. B Biointerfaces 102 (2013) 307-311.

[23] L. Sun, X. Zhou, Y. Zhang, T. Guo, Enhanced field emission of graphene-ZnO quantum dots hybrid structure, J. Alloys Compd. 632 (2015) 604-608.

[24] B.X. Gu, C.X. Xu, G.P. Zhu, S.Q. Liu, L.Y. Chen, M.L. Wang, J.J. Zhu, Layer by layer immobilized horseradish peroxidase on zinc oxide nanorods for biosensing, J. Phys. Chem. B 113 (2009) 6553-6557.

[25] J. Jiang, X. Zhang, P. Sun, L. Zhang, ZnO/BiOI heterostructures: Photoinduced charge-transfer property and enhanced visible-light photocatalytic activity, J. Phys. Chem. C 115 (2011) 20555-20564.

[26] Y.Y. Zhao, P. Deng, Y.X. Nie, P.L. Wang, Y. Zhang, L.L. Xing, X.Y. Xue, Biomolecule-adsorption-dependent piezoelectric output of ZnO nanowire nanogenerator and its application as self-powered active biosensor, Biosen. Bioelectron. 57 (2014) 269-275.

[27] Y. Tong, C. Zheng, W. Lang, F. Wu, T. Wu, W. Luo, H. Chen, ZnO-embedded BiOI hybrid nanoflakes: Synthesis, characterization, and improved photocatalytic properties, Mater. Des. 122 (2017) 90-101.

[28] P. Ju, Y. Xiang, Z. Xiang, M. Wang, Y. Zhao, D. Zhang, J. Yu, X. Han, BiOI hierarchical nanoflowers as novel robust peroxidase mimetics for colorimetric detection of H_2O_2, RSC Adv. 6 (2016) 17483-17493.

[29] D.Y. Zhai, B.R. Liu, Y. Shi, L.J. Pan, Y.Q. Wang, W.B. Li, R. Zhang, G.H. Yu, Highly sensitive glucose sensor based on pt nanoparticle/polyaniline hydrogel heterostructures, ACS Nano 7 (2013) 3540-3546.

[30] L. Ding, M. Zhao, S. Fan, Y. Ma, J. Liang, X. Wang, Y. Song, S. Chen, Preparing Co_3O_4 urchin-like hollow microspheres self-supporting architecture for improved glucose biosensing performance, Sens. Actuators, B: Chem. 235 (2016) 162-169.

[31] L. Yang, C. Xu, F. Wan, H. He, H. Gu, J. Xiong, Synthesis of RGO/BiOI/ZnO composites with efficient photocatalytic reduction of aqueous Cr(VI) under visible-light irradiation, Mater. Res. Bull. 112 (2019) 154–158.

[32] L. Wang, W. Wang, Y. Chen, L. Yao, X. Zhao, H. Shi, M. Cao, Y. Liang, Liang. Heterogeneous p–n Junction CdS/Cu_2O Nanorod Arrays: Synthesis and Superior Visible-Light-Driven Photoelectrochemical Performance for Hydrogen Evolution. ACS Appl. Mater. Interfaces 10 (2018) 11652−11662.

[33] J. Liu, S. Zou, B. Lou, C. Chen, L. Xiao, J. Fan, Interfacial Electronic Interaction Induced Engineering of ZnO-BiOI Heterostructures for Efficient Visible-Light Photocatalysis, Inorg. Chem. 58 (2019) 8525−8532.

[34] A. Wei, X.W. Sun, J.X. Wang, Y. Lei, X.P. Cai, C.M. Li, Z.L. Dong, W. Huang, Enzymatic glucose biosensor based on ZnO nanorod array grown by hydrothermal decomposition, Appl. Phys. Letter. 89 (2006) 123902.

[35] K. Yang, G.W. She, H. Wang, X.M. Ou, X.H. Zhang, C.S. Lee, S.T. Lee, ZnO nanotube arrays as biosensors for glucose, J. Phys. Chem. C 113 (2009) 20169-20172.

[36] T. Kong, Y. Chen, Y. Ye, K. Zhang, Z. Wang, X. Wang, An amperometric glucose biosensor based on the immobilization of glucose oxidase on the ZnO nanotubes, Sens. Actuators, B: Chem. 138 (2009) 344-350.

[37] E.M.I.M. Ekanayake, D.M.G. Preethichandra, K. Kaneto, Polypyrrole nanotube array sensor for enhanced adsorption of glucose oxidase in glucose biosensors, Biosens. Bioelectron. 23 (2007) 107-113.

[38] H. Lee, S.W. Yoon, E.J. Kim, J. Park, In-situ growth of copper sulfide nanocrystals on multiwalled carbon nanotubes and their application as novel solar cell and amperometric glucose sensor materials, Nano Lett. 7 (2007) 778-784.

[39] A. Umar, M.M. Rahman, Y.B. Hahn, MgO polyhedral nanocages and nanocrystals based glucose biosensor, Electrochem. Commun. 11 (2009) 1353-1357.

[40] Y. Zou, C. Xiang, L.X. Sun, F. Xu, Glucose biosensor based on electrodeposition of platinum nanoparticles onto carbon nanotubes and immobilizing enzyme with chitosan-SiO_2 sol-gel, Biosen. Bioelectron. 23 (2008) 1010-1016.

[41] A. Umar, M.M. Rahman, A. Al-Hajry, Y.B. Hahn, Enzymatic glucose biosensor based on flower-shaped copper oxide nanostructures composed of thin nanosheets, Electrochem. Commun. 11 (2009) 278-281.

[42] A. Samphao, P. Butmee, J. Jitcharoen, L. Švorc, G. Raber, K. Kalcher, Flow-injection amperometric determination of glucose using a biosensor based on immobilization of glucose oxidase onto Au seeds decorated on core Fe_3O_4 nanoparticles, Talanta 142 (2015) 35-42.

[43]V. Guzsvány, J. Anojčić, E. Radulović, O. Vajdle, I. Stanković, D.Madarász, Z. K ónya, K. Kalcher, Screen-printed enzymatic glucose biosensor based on a composite made from multiwalled carbon nanotubes and palladium containing particles, Microchim. Acta (2017), 1-10.

[44] T. Huang, Z. Liu, Y. Li, L. Chao, C. Chen, Y. Tan, Q. Xie, S. Yao, Y. Wu, Oxidative polymerization of 5-hydroxytryptamine to physically and chemically immobilize glucose oxidase for electrochemical biosensing, Anal. Chim. Acta. 1013, (2018) 26-35.

Figure captions

Fig. 1. (a) SEM image of the ZnO/Ni foam. (b) High magnification SEM image of the prepared ZnO/Ni foam. (c) High magnification SEM image of the prepared ZnO nanorods decorated on Ni foam. (d) SEM image of the prepared BiOI/ZnO/Ni foam. (e) High magnification SEM image of the BiOI/ZnO/Ni foam. (f) High magnification SEM image of the prepared BiOI/ZnO nanorods decorated on Ni foam. (g) The section of the ZnO/BiOI nanorod. (h) TEM image of the prepared BiOI/ZnO nanorod. (i) Schematic diagram of the BiOI/ZnO/Ni foam.

Scheme 1. Schematic diagram of the BiOI/ZnO/Ni foam for immobilizing enzymes.

Fig. 2. (a) CV curves of the biosensor in the presence and absence of 5 mM glucose in 0.1 M PBS (pH=7.4). (b) The selectivity of biosensors to glucose with DA, AA, UA, and CC. (c) Typical i-t curve of the biosensor with the continuous addition of glucose at 0.3 V. (d) Calibration curve for the glucose concentration versus current. (e) Typical i-t curve of the biosensor with the continuous addition of H_2O_2 at 0.3 V. (f) Schematic illustration of the GOx/BiOI/ZnO/Ni foam for multiple responses and electrons transport.

Fig. 3. The p-n junction impacts of the GOx/BiOI/ZnO/Ni foam on glucose detection.

Figures

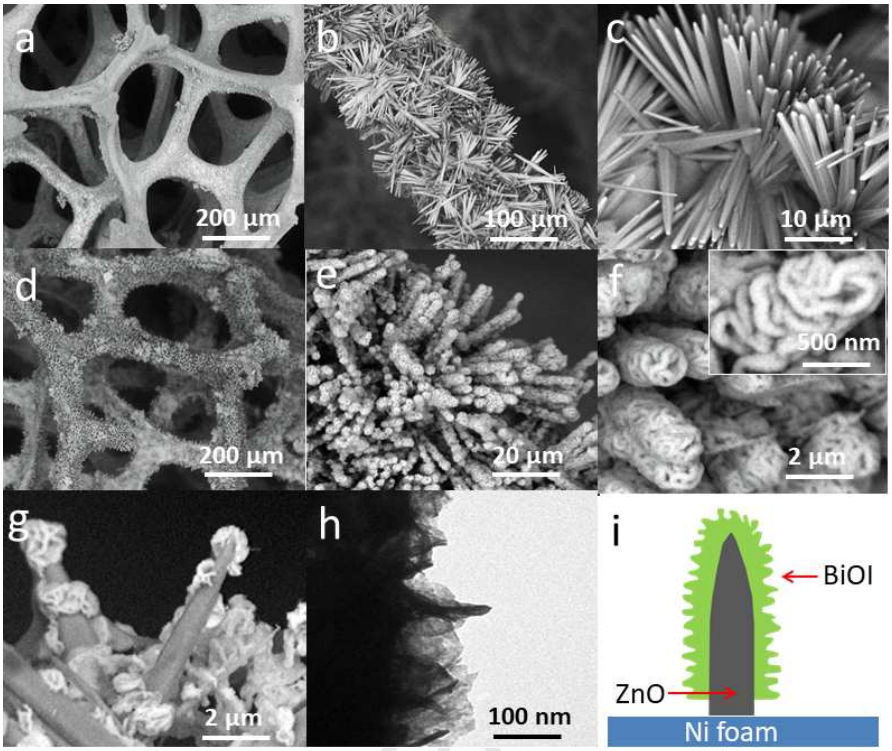

Fig. 1

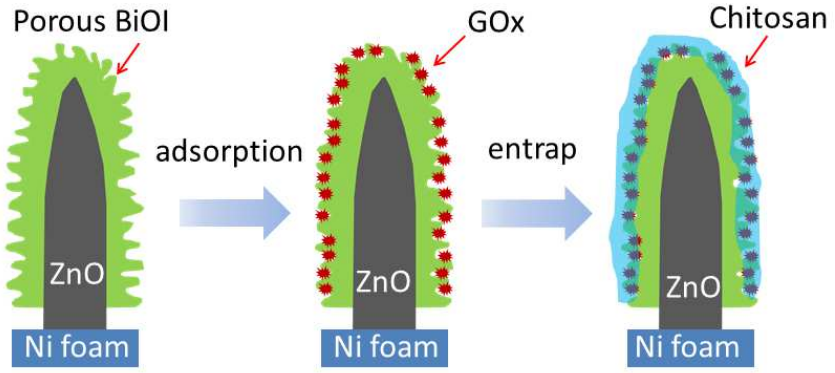

Scheme 1

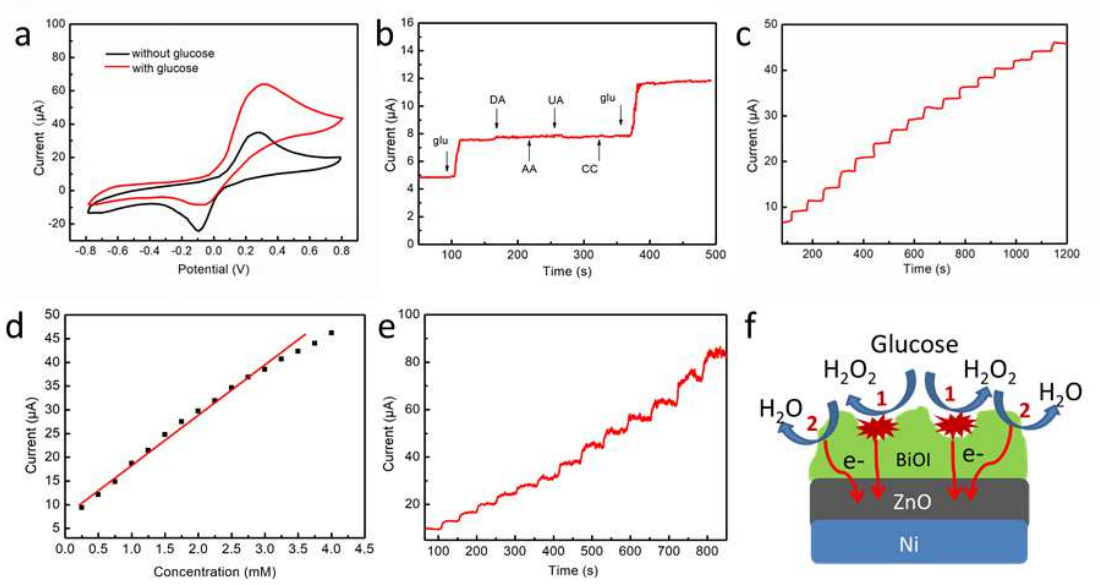
a
without glucose
with glucose
Current (μA)
Potential (V)
b
DA
UA
glu
glu
AA
CC
Current (μA)
Time (s)
c
Current (μA)
Time (s)
d
Current (μA)
Concentration (mM)
e
Current (μA)
Time (s)
f
Glucose
H2O2
H2O2
H2O
H2O
1
1
2
2
e-
BiOI
e-
ZnO
Ni

Fig. 2

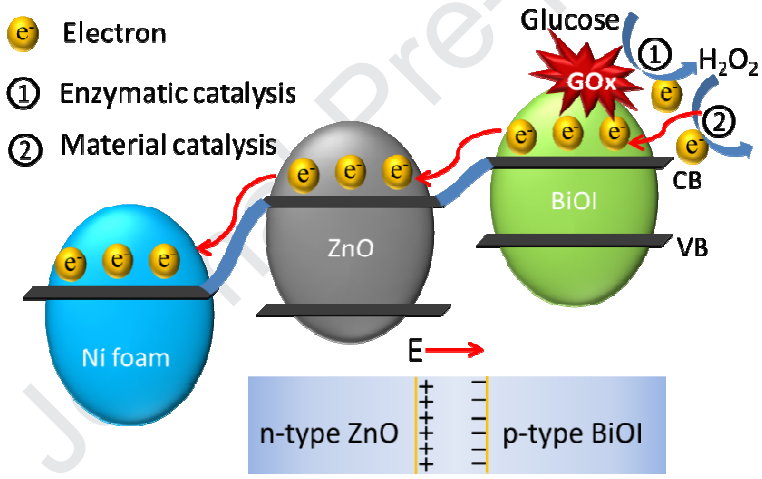
Electron
① Enzymatic catalysis
② Material catalysis
Glucose
GOx
① H2O2
②
CB
VB
BiOI
ZnO
Ni foam
E
n-type ZnO
p-type BiOI

Fig. 3

Tables

Table 1. The performance of various enzymatic biosensors to glucose.

Materials	Potential (V)	Sensitivity ($\mu A \cdot mM^{-1} \cdot cm^{-2}$)	Detection Limit (μM)	Ref.
ZnO nanorod	0.8	23.1	10	[34]
ZnO nanotube	0.8	26.3	10	[35]
ZnO nanotube	0.8	30.85	10	[36]
PPy/Pt	0.4	7.4	30	[37]
Cu_2S-MWCNT	0.55	1.0	10	[38]
MgO nanocages	0.58	31.6	0.68	[39]
SiO_2 sol–gel	0.6	58.9	1	[40]
CuO Flower	0.58	47.19	1.37	[41]
Fe_3O_4@Au/ MnO_2	0.38	2.52	13.2	[42]
Pd-MWCNT	-0.2	18.8	0.997	[43]
5-hydroxytryptamine	0.7	110	0.2	[44]
BiOI/ZnO/Ni foam	0.3	115.2	2	This work

ZnO/BiOI core-shell p-n junction nanorods decorated Ni foam was fabricated and used for glucose detection.

The significantly decreased detection potential (0.3 V) and enhanced sensitivity (115.2 $\mu A \cdot mM^{-1} \cdot cm^{-2}$) were achieved.

The p-n junction foam can afford porous surface, multiple catalysis and accelerated electrons transport.

Declaration of interests

☒ The authors declare that they have no known competing financial interests or personal relationships that could have appeared to influence the work reported in this paper.

☐The authors declare the following financial interests/personal relationships which may be considered as potential competing interests: